J|A|C|S ARTICLES

Published on Web 05/25/2010

# Sulfur K-Edge X-ray Absorption Spectroscopy and Density Functional Calculations on Mo(IV) and Mo(VI)═O Bis-dithiolenes: Insights into the Mechanism of Oxo Transfer in DMSO Reductase and Related Functional Analogues

Adam L. Tenderholt,[†] Jun-Jieh Wang,[‡] Robert K. Szilagyi,[†,⊥] Richard H. Holm,*[,‡] Keith O. Hodgson,*[,†,§] Britt Hedman,*[,§] and Edward I. Solomon*[,†,§]

*Department of Chemistry, Stanford University, Stanford, California 94305, Department of Chemistry and Chemical Biology, Harvard University, Cambridge Massachusetts 02138, and Stanford Synchrotron Radiation Lightsource, SLAC National Accelerator Laboratory, Menlo Park, California 94025*

Received December 11, 2009; E-mail: holm@chemistry.harvard.edu; hodgson@ssrl.slac.stanford.edu; hedman@ssrl.slac.stanford.edu; edward.solomon@stanford.edu

***Abstract:*** Sulfur K-edge X-ray absorption spectroscopy (XAS) and density functional theory (DFT) calculations have been used to determine the electronic structures of two Mo bis-dithiolene complexes, $[Mo(OSi)(bdt)_2]^{1-}$ and $[MoO(OSi)(bdt)_2]^{1-}$, where OSi = $[OSiPh_2{}^tBu]^{1-}$ and bdt = benzene-1,2-dithiolate(2−), that model the Mo(IV) and Mo(VI)═O states of the DMSO reductase family of molybdenum enzymes. These results show that the Mo(IV) complex undergoes metal-based oxidation unlike Mo tris-dithiolene complexes, indicating that the dithiolene ligands are behaving innocently. Experimentally validated calculations have been extended to model the oxo transfer reaction coordinate using dimethylsulfoxide (DMSO) as a substrate. The reaction proceeds through a transition state (TS1) to an intermediate with DMSO weakly bound, followed by a subsequent transition state (TS2) which is the largest barrier of the reaction. The factors that control the energies of these transition states, the nature of the oxo transfer process, and the role of the dithiolene ligand are discussed.

## 1. Introduction

Molybdenum enzymes are present in all forms of life, ranging from ancient bacteria to humans, and with the exception of the nitrogenases, mostly catalyze oxo transfer reactions.[1−3] These Mo "oxotransferases" are divided into three groups based on the protein sequences and structures of the active sites: the DMSO reductase (DMSOr), sulfite oxidase, and xanthine oxidase families. Each member of these families cycle between the Mo(IV) and Mo(VI) oxidation states and contain at least one pyranopterindithiolene ligand. This cofactor is of particular interest because of its dithiolene group which is often associated with noninnocent behavior (i.e., ligand-based oxidation) in metal-dithiolene complexes.[4−9] For example, formally Mo(VI) tris-dithiolene complexes, in fact, have a metal $d^2$ electron configuration.[6] Molybdenum(VI) sites in the DMSOr family are coordinated by two pterindithiolene cofactors, a protein-derived ligand such as serine, cysteine, or selenocysteine, and have an additional strong oxo ligand (Scheme 1a, right).[10,11] These perturbations appear to result in protein sites and synthetic analogues having innocent redox behavior (i.e., metal-based oxidation).[12]

The enzyme representative of the DMSOr family (i.e., DMSO reductase itself) catalyzes oxo transfer from dimethylsulfoxide (DMSO) to a Mo(IV) des-oxo site resulting in a Mo(VI)═O site and dimethylsulfide (DMS). There have been several experimental and computational studies of structural and/or functional inorganic models of this enzyme and their oxo transfer reactions using a variety of substrates.

The first structural analogues of the DMSOr family were metal bis-dithiolenes with a siloxyl ligand modeling the serine ligand: $[M^{IV}(OSi)(bdt)_2]^{1-}$ and $[M^{VI}O(OSi)(bdt)_2]^{1-}$ (Scheme

[†] Stanford University.
[‡] Harvard University.
[§] SLAC National Accelerator Laboratory.
[⊥] Current address: Department of Chemistry and Biochemistry, Montana State University, Bozeman, MT 59717.

(1) Hille, R. *Chem. Rev.* **1996**, *96*, 2757–2816.
(2) Hille, R. *Trends Biochem. Sci.* **2002**, *27*, 360–367.
(3) Romão, M. *Dalton Trans.* **2009**, *2009*, 4053–4068.
(4) Szilagyi, R. K.; Lim, B. S.; Glaser, T.; Holm, R. H.; Hedman, B.; Hodgson, K. O.; Solomon, E. I. *J. Am. Chem. Soc.* **2003**, *125*, 9158–9169.
(5) Ray, K.; George, S. D.; Solomon, E. I.; Wieghardt, K.; Neese, F. *Chem.—Eur. J.* **2007**, *13*, 2783–2797.
(6) Tenderholt, A. L.; Szilagyi, R. K.; Holm, R. H.; Hodgson, K. O.; Hedman, B.; Solomon, E. I. *Inorg. Chem.* **2008**, *47*, 6382–6392.
(7) Sarangi, R.; George, S. D.; Rudd, D. J.; Szilagyi, R. K.; Ribas, X.; Rovira, C.; Almeida, M.; Hodgson, K. O.; Hedman, B.; Solomon, E. I. *J. Am. Chem. Soc.* **2007**, *129*, 2316–2326.
(8) Kapre, R. R.; Bothe, E.; Weyhermüller, T.; George, S. D.; Wieghardt, K. *Inorg. Chem.* **2007**, *46*, 5642–5650.
(9) Banerjee, P.; Sproules, S.; Weyhermüller, T.; George, S. D.; Wieghardt, K. *Inorg. Chem.* **2009**, *48*, 5829–5847.
(10) George, G. N.; Hilton, J.; Temple, C.; Prince, R. C.; Rajagopalan, K. V. *J. Am. Chem. Soc.* **1999**, *121*, 1256–1266.
(11) George, G. N.; Doonan, C. J.; Rothery, R. A.; Boroumand, N.; Weiner, J. H. *Inorg. Chem.* **2007**, *46*, 2–4.
(12) Enemark, J. H.; Cooney, J. J. A.; Wang, J.-J.; Holm, R. H. *Chem. Rev.* **2004**, *104*, 1175–1200.

***Scheme 1.*** (a) Structures of the Mo(IV) and Mo(VI)═O Sites of DMSO Reductase (Left and Right, Respectively); (b) Mo(IV) and Mo(VI)═O Bis-dithiolene Complexes in This Study (Left and Right, Respectively); (c) Mo Tris-dithiolene Complexes in This Study[a]

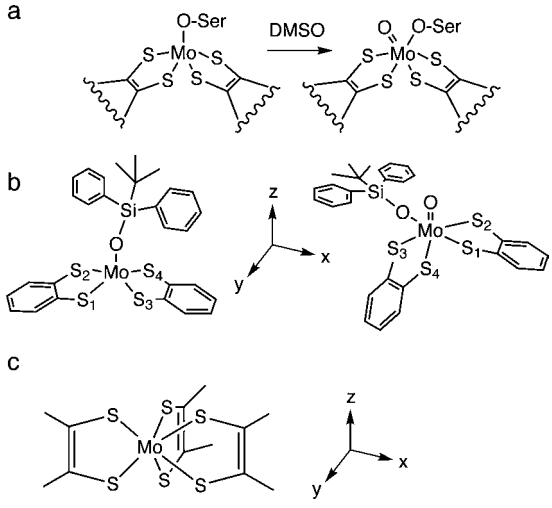


[a] Note that *z*-axis lies along the Mo−O and Mo═O bonds for the Mo(IV) and Mo(VI)═O bis-dithiolenes, respectively, whereas for the Mo tris-dithiolene complexes, the *z*-axis lies along the $C_3$ rotation axis.

1b), where M = Mo or W, OSi = $[OSiPh_2{}^tBu]^{1-}$, and bdt = benzene-1,2-dithiolate(2−).[13] The M(IV) des-oxo complexes exhibit some oxo transfer reactivity, although it proceeds at a slow rate due, at least in part, to the steric bulk of the siloxyl ligand. A more functional set of complexes that replace the axial siloxyl with a phenoxy ligand, that is, [M(OPh)(mdt)] where M = Mo or W and mdt = 1,2-dimethylethene-1,2-dithiolate(2−), has been prepared.[12,14−17] Kinetics parameters of oxo transfer to these M(IV) des-oxo complexes using substrates such as DMSO, $(CH_2)_4SO$, and $(CH_3)_3NO$ (TMNO) were determined and showed that reaction rates are highly substrate-dependent.[16] These studies also demonstrated that oxo transfer to W sites is faster than to the analogous Mo site. Finally, oxo transfer rates from $(CH_2)_4SO$ to W(IV) bis-dithiolenes were determined for a variety of substituents on the axial phenoxy and dithiolene ligands and showed that electron-withdrawing substituents accelerate the reaction.[17] This comprehensive study led to the proposal that the rate-determining step involves W−O (and by extension Mo−O) bond formation and not electron-transfer as it accompanies S−O bond breaking.

Computational studies of oxo transfer on sites that model DMSOr began shortly after the first kinetics experiments. The first study on oxo transfer started from a DMSO-bound Mo(IV) bis-dithiolene intermediate complex.[18] Results from this study led the authors to conclude that the active site in DMSOr is constrained by the protein in a way that decreases both the energy of the transition state and the exothermicity of the reaction. Indeed, a recent spectroscopic and computational study has demonstrated that the structural constraints due to the protein raises the energy of the Mo(IV) bis-dithiolene HOMO, making nucleophilic attack on substrate X−O bonds more favorable, and thus lowers the energy of the transition state.[19] Other computational studies with similar Mo(IV) bis-dithiolenes, as well as W analogues, determined that the reaction coordinate starting from free DMSO has an additional transition state before reaching the DMSO-bound intermediate.[20−22] These studies also calculated that the energy of the largest barrier is lower for W sites compared to Mo (in agreement with experiment) but that this rate-limiting step involves S−O bond breaking, at least for the Mo sites and possibly for the W sites.

Despite the insight into oxo transfer gained from these experimental and computational studies, none have presented the electronic structures of both Mo(IV) and Mo(VI)═O sites (i.e., quantified the metal-dithiolene bonding), the factors that govern the energies along an oxo transfer reaction coordinate, the nature of oxo transfer, or the role of the dithiolene in oxo transfer. The focus of this study is to define the electronic structures (especially the metal-dithiolene bonding) of the Mo(IV) and Mo(VI)═O bis-dithiolenes $[Mo(OSi)(bdt)_2]^{1-}$ and $[MoO(OSi)(bdt)_2]^{1-}$ (Scheme 1b) using S K-edge X-ray absorption spectroscopy (XAS) combined with density functional theory (DFT) calculations and to use these experimentally validated DFT calculations in a detailed investigation of the oxo transfer reaction coordinate. Since ligand K-edge XAS is a direct probe of metal−sulfur bonding[7,23,24] in complexes and enzymes, it is an excellent method for evaluating the metal-dithiolene bonding and its role in the oxo transfer reaction.

Excitation of a S 1s electron into the unoccupied S 4p orbitals and the continuum using tunable synchrotron radiation at an energy around 2474 eV results in an electric-dipole-allowed X-ray absorption K-edge. Transitions to unoccupied valence molecular orbitals with S 3p character are typically observed at energies lower than this edge. The intensity ($D_0$) of these pre-edge features depends upon the amount of S 3p mixing and is given by

$$D_0(\mathrm{S\,1s} \rightarrow \psi^*) = \mathrm{const}\,|\langle \mathrm{S\,1s}|\mathbf{r}|\psi^*\rangle|^2 = \frac{\alpha^2 h}{3n} I_s \qquad (1)$$

where **r** is the electric-dipole operator, $\psi^* = \sqrt{1-\alpha^2}|M_d\rangle - \alpha|S_{3p}\rangle$ (i.e., the antibonding orbital corresponding to the metal−ligand bond), $\alpha^2$ is the covalency (i.e., the amount of sulfur character mixed into the metal d orbitals), *h* is the number of holes in the acceptor orbital to account for potential spin and/or orbital degeneracy, and $I_s$ is the intensity of the electric-dipole allowed S 1s → S 3p transition, which depends upon $Z_{eff}$ and is estimated from the experimental S K-edge data in this study.[7] Note that XAS data is normalized such that the intensity of the post-edge region is 1.0, and thus the factor of *n* in the denominator is included to account for multiple absorbing atoms (i.e., sulfur). Thus, metal−sulfur bonding in Mo bis-dithiolene complexes can be experimentally quantified from the intensity of pre-edge features in S K-edge data and

(13) Donahue, J. P.; Lorber, C.; Nordlander, E.; Holm, R. H. *J. Am. Chem. Soc.* **1998**, *120*, 3259–3260.
(14) Lim, B. S.; Sung, K.-M.; Holm, R. H. *J. Am. Chem. Soc.* **2000**, *122*, 7410–7411.
(15) Lim, B. S.; Holm, R. H. *J. Am. Chem. Soc.* **2001**, *123*, 1920–1930.
(16) Sung, K.-M.; Holm, R. H. *J. Am. Chem. Soc.* **2001**, *123*, 1931–1943.
(17) Sung, K.-M.; Holm, R. H. *J. Am. Chem. Soc.* **2002**, *124*, 4312–4320.
(18) Webster, C. E.; Hall, M. B. *J. Am. Chem. Soc.* **2001**, *123*, 5820–5821.
(19) McNaughton, R. L.; Lim, B. S.; Knottenbelt, S. Z.; Holm, R. H.; Kirk, M. L. *J. Am. Chem. Soc.* **2008**, *130*, 4628–4636.
(20) Thapper, A.; Deeth, R. J.; Nordlander, E. *Inorg. Chem.* **2002**, *41*, 6695–6702.
(21) McNamara, J. P.; Hillier, I. H.; Bhachu, T. S.; Garner, C. D. *Dalton Trans.* **2005**, 3572–3579.
(22) Hofmann, M. *J. Mol. Struct. THEOCHEM* **2006**, *773*, 59–70.
(23) Hedman, B.; Hodgson, K. O.; Solomon, E. I. *J. Am. Chem. Soc.* **1990**, *112*, 1643–1645.
(24) Solomon, E. I.; Hedman, B.; Hodgson, K.; Dey, A.; Szilagyi, R. K. *Coord. Chem. Rev.* **2005**, *249*, 97–129.

correlated to DFT calculations, which are then extended to determine the reaction coordinate of oxo transfer.

## 2. Experimental Section

**2.1. Sample Preparation.** The complexes $[Mo(OSi)(bdt)_2]^{1-}$ and $[MoO(OSi)(bdt)_2]^{1-}$, where OSi = $OSiBu^tPh_2^{1-}$ and bdt = benzene-1,2-dithiolate(2−), were prepared as described in ref 25.

**2.2. X-ray Absorption Measurements and Data Analysis.** Sulfur K-edge data were measured at the Stanford Synchrotron Radiation Laboratory under ring conditions of 3 GeV and 80−100 mA. The measurements utilized the 54-pole wiggler beamline 6-2 operating in high field mode of 10 kG with a Ni-coated harmonic rejection mirror and a fully tuned Si(111) crystal monochromator. Details of the beamline optimization for S K-edge XAS studies have been published elsewhere.[24] The solid samples were ground in an inert atmosphere ($N_2$) dry glovebox at less than 1 ppm $O_2$ and dispersed as thinly as possible on a Mylar tape to minimize the possibility of fluorescence self-absorption effects. A 6 $\mu$m thick, sulfur-free polypropylene window was used to prevent sample exposure to air upon mounting in the sample chamber. The photon energy was calibrated to that of the first pre-edge feature of $Na_2S_2O_3 \cdot 5H_2O$ at 2472.02 eV. Scans were averaged using MAVE, which is part of the EXAFSPAK suite of programs,[26] and a smooth background (second-order polynomial) was subtracted from the average spectrum. Normalization of the S K-edge data was accomplished by fitting the post-edge region with a flat first-order polynomial and scaling the data such that the value of this fit function is 1.0 at 2490 eV. Both background subtraction and normalization were performed using PySpline.[27] Since the post-edge region also contains intensity from the Mo $L_3$-edge, the data were further scaled such that the region between the S K-edge and Mo $L_3$-edge had the same intensity as the corresponding region of a tungsten dithiolene complex. Pre-edge features were modeled by pseudo-Voigt peak shapes using the program EDG_FIT[26] with a fixed 1:1 ratio of Lorentzian to Gaussian contributions and simultaneously fit to both normalized intensity and the second derivative. Error in the total pre-edge peak areas ranges from ∼2% for well-resolved pre-edges to ∼10% for unresolved pre-edges. In addition, normalization procedures can introduce ∼5% error in the total pre-edge peak areas. Conversion between peak area and sulfur covalency was accomplished using eq 1, where $D_0$ is the peak area and $I_s$ was determined according to ref 7. Error in determining $I_s$ from the S 1s → 4p transition results in a ±2−4% deviation in the reported covalency value.

**2.3. Electronic Structure Calculations.** Density functional calculations were performed using the Gaussian 03[28] and ORCA[29] packages. Gaussian calculations were performed using the pure functional BP86 (Becke GGA exchange[30] with Perdew 1986 nonlocal correlation[31]) and the hybrid functional B3LYP[32] (Becke GGA exchange modified to include Hartree−Fock mixing with Lee, Yang, and Parr correlation[33,34]). Both functionals give similar electronic structure descriptions for the stationary states, so only the results from the B3LYP calculations are reported. This functional is also used for the reaction coordinate since energies of states during oxo transfer have smaller errors compared to higher level theory than the BP86 functional.[22] The SDD basis set,[35] which is triple-$\zeta$ quality with an effective core potential (ECP), augmented with additional polarization functions[36] was used for the Mo atoms. The 6-311G(d) basis set was used for sulfur and oxygen atoms, whereas the 6-31G(d) basis set was used for silicon, carbon, and hydrogen atoms. Calculations using the broken symmetry formalism[37] were performed using B3LYP with the DefBas-3 basis functions, which are derived from the Ahlrichs basis sets,[38] for all atoms as implemented in ORCA.

Geometry optimizations and frequency calculations were performed without solvent. No imaginary modes were present for stationary states. Transition states were confirmed to have a single imaginary mode. Single point calculations were performed using the polarized continuum solvent (PCM) method[39] using the default parameters for acetonitrile. QMForge,[40] which utilizes the cclib library[41] for parsing and analyzing logfiles, was used for calculating the composition of molecular orbitals via Mulliken population analysis[42] and for Mayer bond orders.[43,44]

## 3. Results and Analysis

**3.1. Sulfur K-edge XAS.** The sulfur K-edge XAS spectra for the Mo bis-dithiolene complexes in this study are presented in Figure 1. The Mo tris-dithiolene complexes are included for reference as their electronic structures have already been defined.[6] The Mo(IV) complexes (red, top panel) both have significant pre-edge intensity at ∼2471.3 eV. The pre-edge in the Mo(IV) bis-dithiolene complex (solid) has a shoulder at higher energy (2472.2 eV), while the pre-edge in the Mo(IV) tris-dithiolene (dashed) has a small contribution at lower energy (indicated by a asterisk at 2470.2 eV) due to an oxidized impurity (10%, see ref 6). In addition, another unresolved pre-edge feature is present in the data of both the bis- and tris-dithiolene complexes at 2473.2 and 2472.7 eV, respectively. The formally Mo(VI) complexes (blue, bottom panel) both have an additional pre-edge feature at ∼2470.4 eV compared with their Mo(IV) counterparts, which is consistent with an additional unoccupied orbital (two holes) due to oxidation. The formally Mo(VI) tris-dithiolene complex (dashed) has two resolved pre-edges features at 2470.4 and 2471.5 eV, and one unresolved pre-edge feature at ∼2472.9 eV, while the Mo(VI)═O bis-dithiolene complex (solid) has several overlapping peaks in the same energy region. It is important to note that the pre-edge peaks in the formally Mo(VI) tris-dithiolene have more intensity than the corresponding features in the bis-dithiolene (both are normalized to one sulfur).

Representative peak fits (based on simultaneous fits to the second derivative; see Supporting Information) are shown in

(25) Donahue, J. P.; Goldsmith, C. R.; Nadiminti, U.; Holm, R. H. *J. Am. Chem. Soc.* **1998**, *120*, 12869–12881.
(26) George, G. N. *EXAFSPAK*; Stanford Synchrotron Radiaton Laboratory: Menlo Park, CA, 1990.
(27) Tenderholt, A. L.; Hedman, B.; Hodgson, K. O. *AIP Conf. Proc.* **2006**, *882*, 105–107.
(28) Frisch, M. J. et al., *Gaussian 03, revisions C.01 and E.01*; Gaussian, Inc.: Wallingford, CT, 2004.
(29) Neese, F. *ORCA−An Ab-initio, DFT and Semiempirical Electronic Structure Package, version 2.6 revision 35*; Institut fr Physikalische und Theoretische Chemie: Universitt Bonn, Germany, 2004.
(30) Becke, A. D. *Phys. Rev. A* **1988**, *83*, 3098–3100.
(31) Perdew, J. P. *Phys. Rev. B* **1986**, *33*, 8822–8824.
(32) Becke, A. D. *J. Chem. Phys.* **1993**, *98*, 5648–5652.
(33) Lee, C.; Yang, W.; Parr, R. G. *Phys. Rev. B* **1988**, *37*, 785–789.
(34) Miehlich, B.; Savin, A.; Stoll, H.; Preuss, H. *Chem. Phys. Lett.* **1989**, *157*, 200–206.
(35) Andrae, D.; Häussermann, U.; Dolg, M.; Stoll, H.; Preuss, H. *Theor. Chim. Acta* **1990**, *77*, 123–141.
(36) Ehlers, A.; Böhme, M.; Dapprich, S.; Gobbi, A.; Höllwarth, A.; Jonas, V.; Khler, K.; Stegmann, R.; Veldkamp, A.; Frenking, G. *Chem. Phys. Lett.* **1993**, *208*, 111–114.
(37) Neese, F. *J. Phys. Chem. Solids* **2004**, *65*, 781–785.
(38) Schkifer, A.; Horn, H.; Ahlrichs, R. *J. Chem. Phys.* **1992**, *97*, 2571–2577.
(39) Tomasi, J.; Mennucci, B.; Cammi, R. *Chem. Rev.* **2005**, *105*, 2999–3094.
(40) Tenderholt, A. L. *QMForge, v. 2.1*; Stanford University: Stanford CA, 2007; http://qmforge.sourceforge.net.
(41) O'Boyle, N. M.; Tenderholt, A. L.; Langner, K. M. *J. Comput. Chem.* **2008**, *29*, 839–845.
(42) Mulliken, R. *J. Chem. Phys.* **1955**, *23*, 1833–1840.
(43) Mayer, I. *Chem. Phys. Lett.* **1983**, *97*, 270–274.
(44) Bridgeman, A. J.; Cavigliasso, G.; Ireland, L. R.; Rothery, J. *J. Chem. Soc., Dalton Trans.* **2001**, 2095–2108.

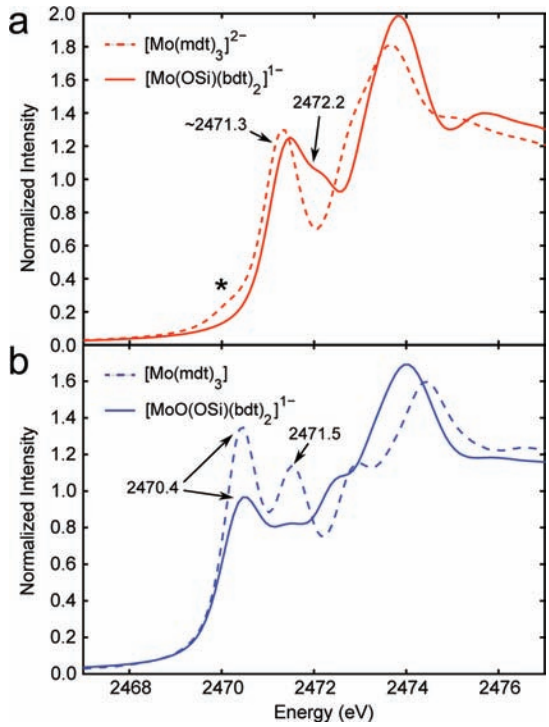


***Figure 1.*** Normalized S K-edge XAS data of (a) Mo(IV) tris- and bis-dithiolene (dashed and solid red, respectively) and (b) formally Mo(VI) tris- and Mo(VI)═O bis-dithiolene (dashed and solid blue, respectively) complexes. The asterisk marks the oxidized impurity in the Mo(IV) tris-dithiolene complex.

Figure 2 and the parameters obtained from the fits are in Table 1. For the Mo tris-dithiolene complexes (dashed lines), the resolved pre-edges at ~2470.4 and ~2471.4 eV were assigned as S 1s → ligand $\pi^{+}_{AB}$ (Scheme 2a) and S 1s → Mo $d_{x^2-y^2}/d_{xy}$ transitions, respectively (coordinate system for trigonal prismatic geometry defined such that the *z* axis is along the $C_3$ rotation axis).[6] The unresolved pre-edges at 2472.8 eV are assigned as S 1s → Mo $d_{xz}/d_{yz}$ transitions. Finally, the pre-edge features above 2473 eV (dotted gray in Figure 2) are assigned as S 1s → C−S $\pi^*$ transitions as in our previous literature.[4]

For the Mo bis-dithiolene complexes, density functional theory (DFT) calculations (section 3.2) are used to aid peak assignment. The three pre-edge peaks in the Mo(IV) bis-dithiolene complex (Figure 2c, solid red) are assigned as follows. The lowest-energy pre-edge (i.e., 2471.4 eV) is assigned as S 1s → Mo $d_{xz}/d_{yz}$ transitions, while the pre-edge peaks at 2472.2 and 2473.2 eV are assigned as the S 1s → Mo $d_{z^2}$ and Mo $d_{xy}$ transitions, respectively (coordinate system shown in Scheme 1b). Finally, the pre-edge feature at 2473.9 eV (dotted gray) is assigned as S 1s → C−S $\pi^*$ transitions.

For the Mo(VI)═O bis-dithiolene complex (Figure 2d, solid blue), the pre-edge peak at 2470.4 eV is assigned as S 1s → Mo $d_{x^2-y^2}$ transitions (coordinate system shown in Scheme 1b). As in the Mo(IV) bis-dithiolene complex, the pre-edge at 2471.4 eV is assigned as S 1s → Mo $d_{xz}/d_{yz}$ transitions. It is interesting that this pre-edge peak occurs at about the same energy in both complexes since the d manifold, and thus the pre-edge, should be stabilized to lower energy in the Mo(VI)═O complex due to the higher oxidation state. This indicates that the $\pi$ bonding to the strong axial oxo ligand compensates by destabilizing the Mo $d_{xz}/d_{yz}$ orbitals. The higher-energy pre-edge peaks at 2472.4 and 2473.3 eV are assigned as S 1s → Mo $d_{xy}$ and $d_{z^2}$ transitions, respectively, which is opposite of the order seen in the Mo(IV) bis-dithiolene complex. This is due to the strong oxo axial ligand in the Mo(VI)═O complex compared to the weaker siloxyl in the Mo(IV) complex. Finally, the pre-edge feature at 2473.9 eV (dotted gray in Figure 2) is assigned as S 1s → C−S $\pi^*$ transitions.

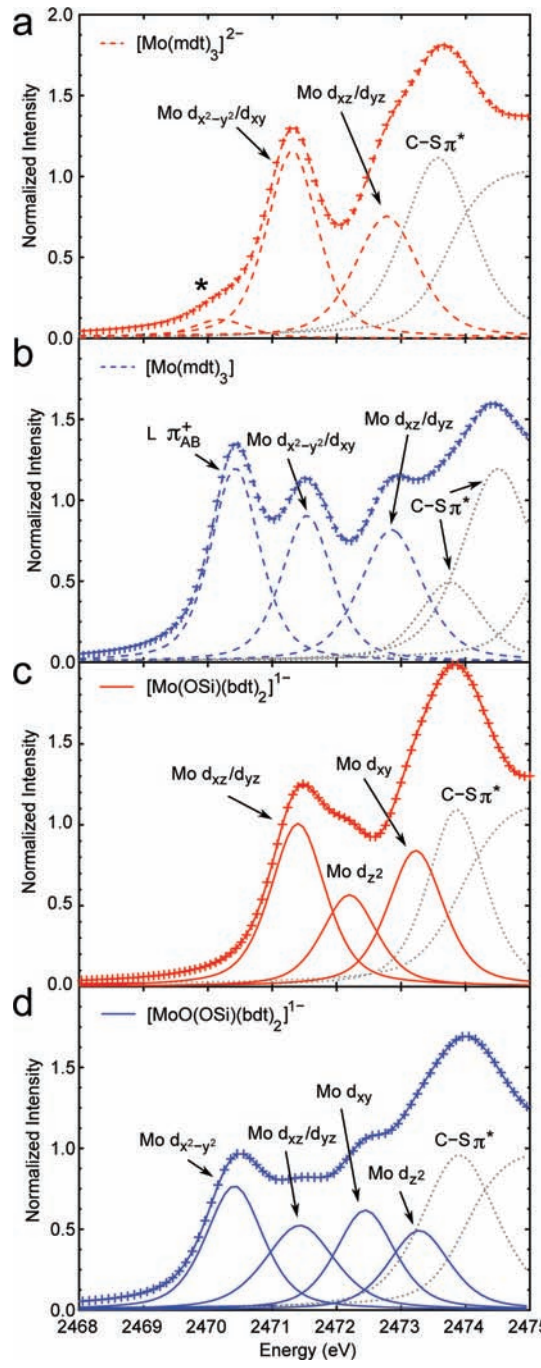


***Figure 2.*** Representative peak fits of the S K-edge data for the (a) Mo(IV) tris-dithiolene, (b) formally Mo(VI) tris-dithiolene, (c) Mo(IV) bis-dithiolene, and (d) Mo(VI)═O bis-dithiolene complexes. Data are denoted as crosses and fits as solid or dashed lines. The asterisk in panel a is due to an oxidized impurity. Peaks due to transitions to the C−S $\pi^*$ orbitals and the rising edge are in dotted gray.

Sulfur K-edge transition intensities were used to experimentally determine the amount of sulfur character in molecular orbitals (Table 1). For the $d^2$ Mo(IV) tris-dithiolene, the resolved (2471.3 eV) and overlapping (2472.7 eV) peaks have 33% and 27% S p character, respectively. This corresponds to a total

***Table 1.*** Pre-edge Peak Energies (*E*), Relative Energies (RE), Intensities ($D_0$), Number of Holes in Respective Orbital (*h*), and Covalencies (i.e., % S p Character) of the S K-edge Data (Figure 2) and Relative Energies and Covalencies As Determined by DFT for the Mo Tris- and Bis-dithiolene Complexes

| | | S K-edge XAS | | | | | DFT | |
|---|---|---|---|---|---|---|---|---|
| | | *E* (eV) | RE (eV) | $D_0$ | *h* | S p (%) | RE (eV) | S p (%) |
| $[Mo(mdt)_3]^{2-}$ | $d_{x^2-y^2}/d_{xy}$ | 2471.31 | | 1.09 | 4 | 33 | | 38 |
| | $d_{xz}/d_{yz}$ | 2472.71 | 1.4 | 0.88 | 4 | 27 | 1.5 | 41 |
| $[Mo(mdt)_3]$ | $\pi^+_{AB}$ | 2470.43 | | 1.09 | 2 | 69 | | 54 |
| | $d_{x^2-y^2}/d_{xy}$ | 2471.54 | 1.1 | 0.85 | 4 | 26 | 1.0 | 42 |
| | $d_{xz}/d_{yz}$ | 2472.85 | 2.3 | 0.94 | 4 | 29 | 2.3 | 40 |
| $[Mo(OSi)(bdt)_2]^{1-}$ | $d_{xz}/d_{yz}$ | 2471.40 | | 1.02 | 4 | 20 | | 23[a] |
| | $d_{z^2}$ | 2472.16 | 0.8 | 0.57 | 2 | 23 | 0.6 | 18 |
| | $d_{xy}$ | 2473.24 | 1.8 | 0.87 | 2 | 35 | 1.9 | 45 |
| $[MoO(OSi)(bdt)_2]^{1-}$ | $d_{x^2-y^2}$ | 2470.41 | | 0.81 | 2 | 32 | | 32 |
| | $d_{xz}/d_{yz}$ | 2471.43 | 1.0 | 0.67 | 4 | 13 | 0.9 | 13[a] |
| | $d_{xy}$ | 2472.44 | 2.0 | 0.67 | 2 | 27 | 2.1 | 35 |
| | $d_{z^2}$ | 2473.28 | 2.9 | 0.55 | 2 | 22 | 3.4 | 23 |

[a] Average of two orbitals.

***Scheme 2.*** Ligand $\pi^+_{AB}$ Orbitals of (a) Mo Tris-dithiolenes and (b) Mo(IV) Bis-dithiolene[a]

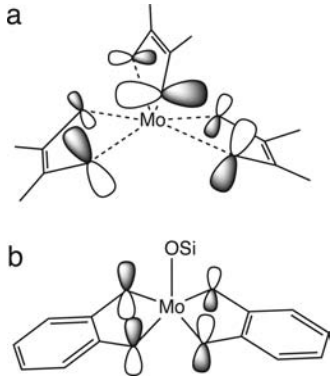


[a] Note that this orbital for the Mo(VI)═O bis-dithiolene is similar to that of the Mo(IV) bis-dithiolene, but with one dithiolene plane rotated relative to the other.

(eight-hole) covalency of 240% S p since these peaks are due to S 1s → Mo $d_{x^2-y^2}/d_{xy}$ and $d_{xz}/d_{yz}$ transitions. The resolved peaks at 2470.4 and 2471.5 eV in the formally $d^0$ Mo(VI) tris-dithiolene have 69% and 26% S p character, respectively, while the overlapping peak at 2472.9 eV has 29% S p character for a total (ten-hole) covalency of 358%. Therefore, in going from the Mo(IV) to the formally Mo(VI) tris-dithiolene, there is an increase of 118% S p character due to two additional holes in the valence molecular orbitals which indicates ligand-based oxidations. Note that this increase corresponds to ~180% dithiolene character since the ligand $\pi^+_{AB}$ (Scheme 2a) orbital is calculated to have a composition of 53% S and 32% C/H.

For the $d^2$ Mo(IV) bis-dithiolene complex, the resolved peaks at 2471.4 and 2472.2 eV have 20% and 23% S p character, respectively, while the overlapping peak at 2473.2 eV has 35% S p character. This corresponds to a total (eight-hole) covalency of 196% S p since these peaks correspond to S 1s → Mo $d_{xz}/d_{yz}$, $d_{z^2}$, and $d_{xy}$ transitions. In contrast to the formally $d^0$ Mo(VI) tris-dithiolene, the $d^0$ Mo(VI)═O bis-dithiolene complex has a total (ten-hole) covalency of 214% S 3p character due to the resolved peak at 2470.4 eV (32% S p) and the overlapping peaks at 2471.4, 2472.4, and 2473.3 eV (13%, 27%, and 22% S p, respectively). This is only an increase of 18% S p character in the $d^0$ Mo(VI)═O bis-dithiolene relative to the $d^2$ Mo(IV) bis-dithiolene due to the two extra holes in the former complex (compared to 118% in the tris-dithiolene). These results show that despite the highly covalent Mo-dithiolene interaction, the Mo(IV) bis-dithiolene complex undergoes metal-based oxidation unlike the Mo tris-dithiolene system.

**3.2. DFT Calculations and Correlation to XAS Data.** Spin-unrestricted DFT calculations were used to gain further insight into the electronic structures of the Mo bis-dithiolene complexes. The electronic structures of the tris-dithiolenes from ref 6 are included for comparison. Geometry optimizations resulted in structural parameters in good agreement with those obtained from X-ray crystallography (see Supporting Information). Molecular orbital diagrams for the complexes are presented in Figure 3. The orbital splitting patterns of the five Mo d and the redox-active orbital for the Mo(IV) and formally Mo(VI) tris-dithiolene complexes (far left and far right, respectively) are divided into four groups as described in ref 6: Mo nonbonding (i.e., Mo $d_{z^2}$), dithiolene $\pi^+_{AB}$ (redox-active, ligand-based orbital shown in Scheme 2a), Mo $\pi$ antibonding (i.e., Mo $d_{x^2-y^2}/d_{xy}$), and Mo $\sigma$ antibonding (i.e., $d_{xz}/d_{yz}$).[6] It is important to note that the Mo $d_{z^2}$ orbital remains occupied in the calculations despite oxidation to the formally Mo(VI) complex, in agreement with the results from S K-edge XAS experiments summarized above.

The orbital splitting pattern of the five-coordinate, square pyramidal Mo(IV) bis-dithiolene complex (Figure 3, center left) is similar to that of the six-coordinate Mo(IV) tris-dithiolene. Both the predominately nonbonding Mo $d_{x^2-y^2}$ (*x* and *y* axes are defined as bisecting the Mo−S bonds, Scheme 1b) and the dithiolene $\pi^+_{AB}$ orbital (Scheme 2b) are occupied, although the Mo $d_{x^2-y^2}$ orbital is now higher in energy. The orbitals with $\pi$-interactions (i.e., Mo $d_{xz}/d_{yz}$) are only slightly split due to different S−Mo−S angles (chelating vs interligand). The major difference compared to the Mo(IV) tris-dithiolene is the 1.3 eV splitting of the $\sigma$-bonding orbitals in the bis-dithiolene (i.e., $d_{xy}/d_{z^2}$) that is observed experimentally (Figure 2a vs Figure 2c).

In going to the Mo(VI)═O bis-dithiolene complex (Figure 3, center right), there are a few noteworthy changes compared to the Mo(IV) bis-dithiolene (center left). The Mo $d_{x^2-y^2}$ orbital is now unoccupied due to the two-electron oxidation, which is in contrast to the formally Mo(VI) tris-dithiolene that has two holes in the ligand $\pi^+_{AB}$ (far right). The orbitals with $\pi$ interactions (i.e., Mo $d_{xz}/d_{yz}$) are split more in the Mo(VI)═O versus Mo(IV) bis-dithiolene because of the axial distortion of one dithiolene upon going to the six-coordinate pseudo-octahedral structure (Scheme 1b, right). The energetic ordering of orbitals with $\sigma$-interactions (i.e., Mo $d_{xy}/d_{z^2}$) are reversed compared to the Mo(IV) bis-dithiolene complex due to the strong axial interaction between the Mo $d_{z^2}$ and the oxo $p_z$ and

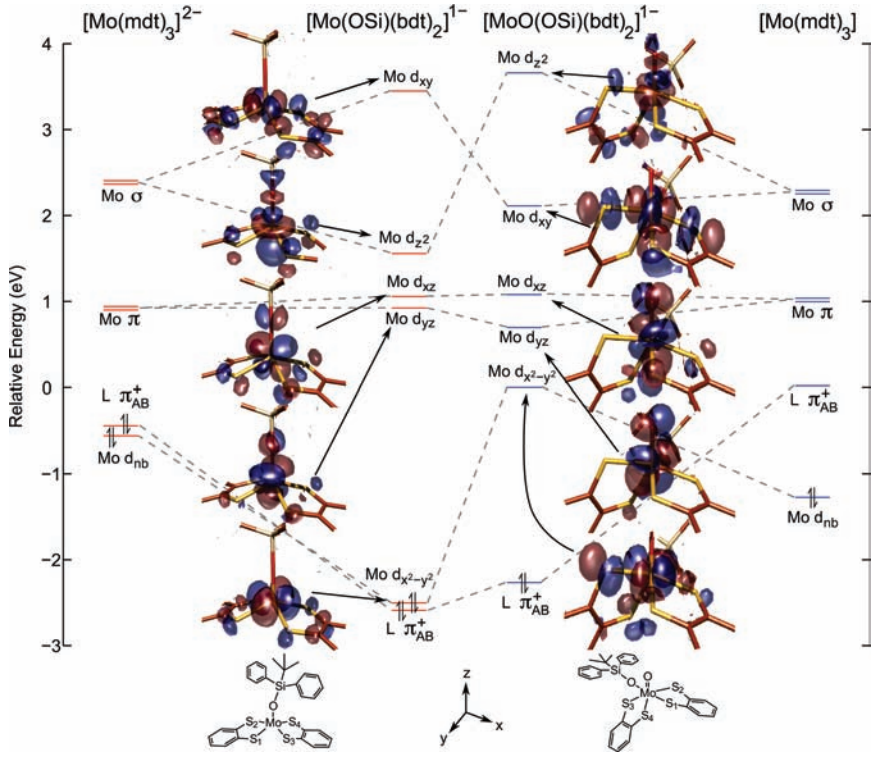


***Figure 3.*** Molecular orbital diagram of the Mo bis- and tris-dithiolene complexes. The tris-dithiolene complexes (far left and far right) adopt a trigonal prismatic structure with the *z*-axis defined along the $C_3$ rotation axis. The Mo(IV) bis-dithiolene complex (middle left) is a square pyramid with the *z*-axis defined along the Mo−O(Si) bond and the *x*-axis bisecting the S−Mo−S chelate angle. The Mo(VI)═O bis-dithiolene (middle right) is distorted octahedral with the *z*-axis along the Mo═O bond and the *x*-axis bisecting the S−Mo−S chelate angle of the dithiolene *cis* to the oxo ligand. Note that some carbon and hydrogen atoms have been removed from the orbital pictures for clarity and that energy levels are shifted so that the relative LUMO energies reflect the differences seen in the S K-edge data.

the loss of one Mo−S bond in the *xy* plane (stabilizes the Mo $d_{xy}$ orbital) as the Mo(VI)═O complex adopts a six-coordinate, pseudo-octahedral structure. This reversal of orbital ordering can be seen experimentally from the relative intensities of these peaks in the Mo(VI)═O bis-dithiolene (0.67 for $d_{xy}$ vs 0.55 for $d_{z^2}$) compared to those of the Mo(IV) bis-dithiolene (0.87 for $d_{xy}$ vs 0.57 for $d_{z^2}$).

The calculated sulfur characters of the unoccupied orbitals can now be compared to the experimental values (Table 1). This has already been discussed in detail for the Mo tris-dithiolenes in ref 6; however, there are three important results worth emphasizing. First, both the $\pi$ and $\sigma$ antibonding sets (i.e., $d_{x^2-y^2}$/$d_{xy}$ and $d_{xz}$/$d_{yz}$, respectively) are calculated to be metal-based in agreement with experiment. Second, the ligand $\pi^{+}_{AB}$ orbital is calculated to have 54% S p character in the formally Mo(VI) tris-dithiolene indicating ligand-based holes. Finally, the change in total calculated sulfur character in going from the Mo(IV) to the formally Mo(VI) tris-dithiolene (316% to 436%, or an increase of 120%) is in good agreement with the change observed experimentally (118%, section 3.1) further supporting an electronic structure description where the Mo(IV) tris-dithiolene undergoes ligand-based oxidation. Note that this 120% increase in S character corresponds to an increase of ~180% dithiolene character since the ligand $\pi^{+}_{AB}$ orbital has a composition of 53% S and 32% C/H.

For the Mo(IV) bis-dithiolene, the lowest energy pre-edge feature appears at 2471.4 eV (Table 1) and is assigned as transitions to the Mo $d_{xz}$/$d_{yz}$ orbitals. These orbitals have $\pi$ antibonding interactions with both out-of-plane dithiolene and siloxyl oxygen p orbitals and are calculated to be split by ~0.2 eV due to the different S−Mo−S angles (i.e., chelating vs interligand). This also causes the Mo $d_{xz}$ and $d_{yz}$ orbitals to have different calculated S characters (26% and 19%, respectively) with the average value (23%) in agreement with experiment (20%). It is noteworthy that this covalency is less than in the corresponding $\pi$ antibonding orbitals of the Mo(IV) tris-dithiolene (i.e., 38%) due to the loss of a dithiolene ligand. The Mo $d_{z^2}$ orbital, which also has $\pi$ antibonding interactions with out-of-plane S orbitals, is calculated to be 0.6 eV higher in energy than the Mo $d_{xz}$/$d_{yz}$ orbitals due to the $\sigma$ antibonding interaction with the siloxyl O $p_z$ orbital. The calculated S p character of 18% is somewhat less than that determined for the pre-edge feature at 2472.2 eV (23%). Finally, the pre-edge feature at 2473.2 eV is assigned as transitions to the Mo $d_{xy}$ orbital, which is calculated to be 1.3 eV higher in energy than the Mo $d_{z^2}$ orbital compared with the experimental splitting of 1.0 eV for the $\sigma$ antibonding orbitals. The Mo $d_{xy}$ orbital has a calculated S character of 45%, which is slightly more than the experimental value (35%); this difference could be due to error in resolution of the overlapping pre-edge peaks. It is interesting that the Mo $d_{xy}$ orbital has a covalency similar to that of the $d_{xz}$/$d_{yz}$ orbitals of the Mo(IV) tris-dithiolene (41%) despite having one less dithiolene and indicates that the Mo−S interaction in this orbital is stronger than for the analogous $\sigma$ antibonding orbitals of the tris-dithiolene. This stronger antibonding interaction is also reflected in the pre-edge peak energies: 2473.2 eV in the bis-dithiolene compared with 2472.7 eV in the tris-dithiolene.

For the Mo(VI)═O bis-dithiolene complex, the lowest energy pre-edge peak at 2470.4 eV (Table 1) can be assigned as transitions to the Mo $d_{x^2-y^2}$ orbital (Figure 2d). It is calculated to have 32% S p character, which is in excellent agreement

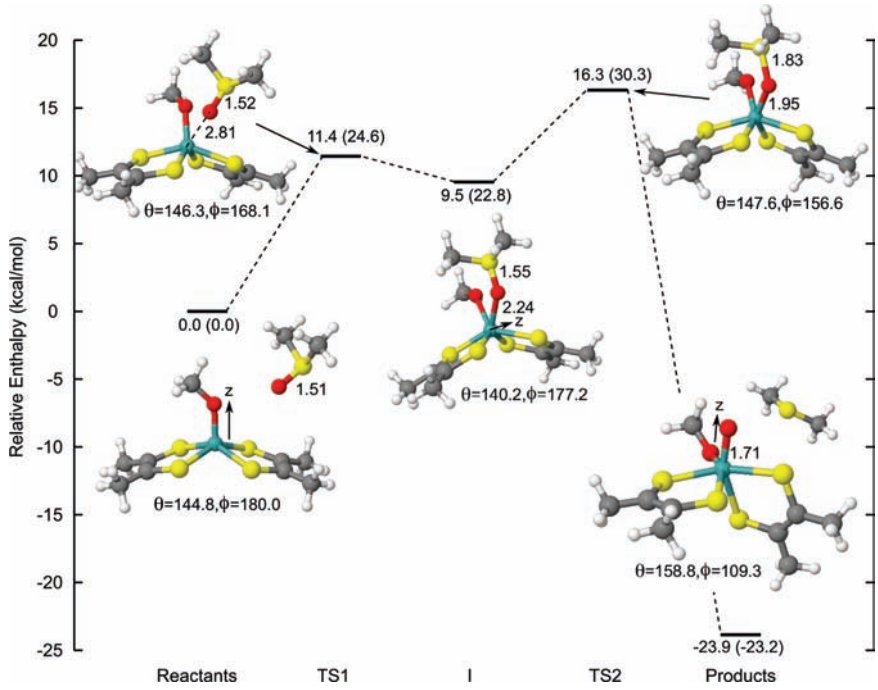


***Figure 4.*** Reaction coordinate of oxo transfer from DMSO to a Mo(IV) bis-dithiolene complex. Values in parentheses are Gibbs free energies. Note that the coordinate system changes in going from the reactants (*z* axis along the Mo−O bond) to the intermediate (*z* axis along the $C_3$ axis) to the products (*z* axis along the Mo═O bond).

with the experimental value (32%). This orbital is nonbonding in the Mo(IV) bis-dithiolene but can now interact with the $\pi^{+}_{AB}$ orbital of the dithiolene that has an axial Mo−S bond due to the distorted octahedral structure (Scheme 1b). The Mo $d_{xz}$ and $d_{yz}$ orbitals, which have $\pi$ antibonding interactions with the dithiolene out-of-plane and oxo p orbitals, are about 0.9 eV higher in energy than the Mo $d_{x^2-y^2}$ orbital. The calculated S p characters for the Mo $d_{xz}$ and $d_{yz}$ orbitals are 17% and 8%, respectively, with an average value (13%) that is in agreement with the experimental value for the pre-edge feature at 2471.4 eV (i.e., 13%). This is less than the corresponding orbitals of the Mo(IV) bis-dithiolene complex and reflects the distortion (a dithiolene with an axial Mo−S bond) required in going to a six-coordinate complex. The next pre-edge feature at 2472.4 eV is assigned as transitions to the Mo $d_{xy}$ orbital and is calculated to have 35% S p character, which is somewhat larger than the experimental value of 27%. This orbital is stabilized relative to the corresponding orbital in the Mo(IV) bis-dithiolene due to both the larger metal $Z_{eff}$, that is, Mo(VI) vs Mo(IV), and the loss of a Mo−S $\sigma$ antibonding interaction in the six-coordinate complex. The pre-edge peak at 2473.3 eV is due to transitions to the Mo $d_{z^2}$ orbital and is calculated to be destabilized by 1.3 eV relative to the Mo $d_{xy}$ orbital due to the strong $\sigma$ antibonding interaction with the oxo $p_z$ orbital. This calculated splitting of the $\sigma$ antibonding orbitals is somewhat larger than the experimental value of 0.9 eV. Finally, the calculated S p character (23%) of the Mo $d_{z^2}$ orbital is also in good agreement with the experimental value (22%).

The change in total calculated covalency in going from the Mo(IV) to the Mo(VI)═O bis-dithiolene (216% to 230%, or an increase of 14%) is in good agreement with the change observed experimentally (18%, section 3.1). It is important to note the total change is significantly less than the change calculated for the tris-dithiolene complexes (118%). This further supports an electronic structure description where the Mo(IV) bis-dithiolene undergoes metal-based oxidation (i.e., innocent redox behavior) despite the highly covalent interaction between Mo and the dithiolene ligands.

**3.3. Oxo Transfer Reaction Coordinate.** Sulfur K-edge XAS and DFT calculations show that the dithiolenes in the Mo(IV) and Mo(VI)═O bis-dithiolene complexes have innocent behavior, despite the highly covalent metal−ligand interactions.[45] These complexes model the reduced and oxidized active sites of the DMSO reductase family of molybdoenzymes. DFT calculations, which have been validated by comparison to experiment in the previous section, are now extended to evaluate the reaction coordinate of oxo transfer. For performance reasons, the Mo(IV) and Mo(VI)═O bis-dithiolene complexes have been truncated to $[Mo(OMe)(mdt)_2]^{1-}$ and $[MoO(OMe)(mdt)_2]^{1-}$, respectively, where OMe = $CH_3O^{1-}$ and mdt =1,2-dimethylethene-1,2-dithiolate(2−).[46] Both of these truncated models have calculated geometric and electronic structures that are similar to those of the untruncated complexes and thus are appropriate models for studying the reaction coordinate (Supporting Information). Furthermore, these models are similar to those used for kinetics experiments and previous computational studies of the oxo transfer reaction coordinate.[14−18,20−22]

Figure 4 presents the reaction coordinate of oxo transfer from DMSO to the Mo(IV) bis-dithiolene complex. In addition to bond lengths, there are two angles that describe changes in the coordination geometry of the dithiolene ligands during the

(45) Note that innocent behavior of Mo(IV) and Mo(VI)═O complexes of mdt and related non-aromatic ligands has been inferred from structural data, which indicate C−S single bonds and C═C double bonds.[12] This is less readily done with bdt complexes owing to the delocalized nature of the ligand. Among other evidence, the non-innocent proclivity of the bdt-type ligand is revealed by the existence of the electron transfer series $[Ni(3,5\text{-}Bu_2{}^tC_6H_2S_2)_2]^z$ where $z$ = 2−, 1−, 0. Sellman, D.; Binder, H.; Hussinger, D.; Heinemann, F. W.; Sutter, J. *Inorg. Chim. Acta* **2000**, *300*−*302*, 829–836.

(46) The complexes $[M(OMe)(mdt)_2]^{1-}$ (M = Mo, W) and [WO(OMe)-$(mdt)_2]^{1-}$ have been prepared and are structurally very similar to $[Mo(OSi)(bdt)_2]^{1-}$ and $[MoO(OSi)(bdt)_2]^{1-}$, respectively. Wang, J.-J.; Tessier, C.; Holm, R. H. *Inorg. Chem.* **2006**, *45*, 2979–2988.

***Scheme 3.*** (a) Angles Used To Describe the Coordination Geometry of the Dithiolenes Ligands; (b) Diagrams of Square Pyramidal and Octahedral Geometries

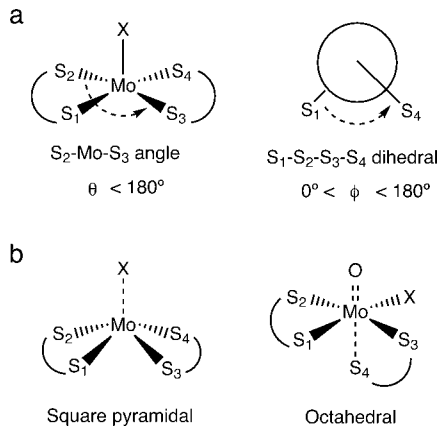


course of the reaction (Scheme 3).[18] For a square pyramidal geometry, which is the structure of the Mo(IV) bis-dithiolene, the $S_1-S_2-S_3-S_4$ dihedral angle is 180°, while the $S_2-Mo-S_3$ angle is less than 180°. For an octahedral geometry, which best describes the structure of the Mo(VI)═O bis-dithiolene, the $S_1-S_2-S_3-S_4$ dihedral angle is 90° and the $S_2-Mo-S_3$ angle is 180°.

The reaction coordinate in Figure 4 first proceeds through a transition state (TS1) with a long (DMS)O−Mo distance (2.81 Å) and a slightly longer DMSO S−O bond compared to that calculated for free DMSO (1.52 vs 1.51 Å). The OMe ligand is distorted away from the axial position to accommodate the incoming DMSO, and there is a slight decrease in the dihedral angle $\phi$ from 180° to 168.1°. This barrier has an enthalpy of 11.4 kcal/mol and free energy of 24.6 kcal/mol. Upon going to the "DMSO-bound" intermediate (I), the (DMS)O−Mo distance decreases to 2.24 Å and the DMSO S−O bond length increases slightly to 1.55 Å. The intermediate also becomes more "trigonal prismatic" as seen by the increase in the dihedral angle $\phi$ from 168.1° to 177.2°. The reaction then proceeds through a second transition state (TS2), which is the largest barrier of the reaction ($\Delta H^{\ddagger}$ = 16.3 and $\Delta G^{\ddagger}$ = 30.3 kcal/mol), and has good agreement with the experimentally determined activation enthalpy (14.9 kcal/mol).[14] The structure has a long DMSO S−O bond (1.83 Å) and a (DMS)O−Mo distance (1.95 Å) that is slightly longer than that seen in complexes with Mo−OR bonds (∼1.9 Å). It is also distorted toward $O_h$ symmetry ($\phi$ = 156.6°). Finally, the product Mo(VI)═O bis-dithiolene has a Mo═O bond length of 1.71 Å and the angles $\phi$ and $\theta$ are 109.3° and 158.8°, respectively, indicating a structure that is distorted octahedral. These results are in agreement with the calculated reaction coordinates of oxo transfer from previous studies.[18,21,22]

Mayer bond orders (Figure 5) provide insight into the electronic structure changes that accompany these geometric changes. The Mo−O(Me) and DMSO S−O bond orders are calculated to be 1.0 and 1.5, respectively, in the reactants. At the first transition state (TS1), the DMSO S−O bond order decreases to 1.3 while a (DMS)O−Mo bond starts to form (bond order of 0.3). Since the S−O bond length is only slightly longer, these changes represent initial charge donation from the S−O bond to the Mo complex. Consistent with the formation of a weaker sixth bond, the Mo−O(Me) bond order also decreases to 0.8. These changes continue upon going to the DMSO-bound intermediate (I): the DMSO S−O bond order decreases to 1.1, the (DMS)O−Mo bond order increases to 0.5, and the

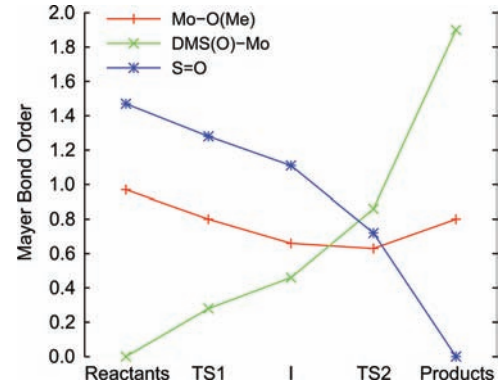


***Figure 5.*** Mayer bond orders for the Mo−O(Me) (red), DMS(O)−Mo (green), and S═O (blue) bonds during the oxo transfer reaction coordinate.

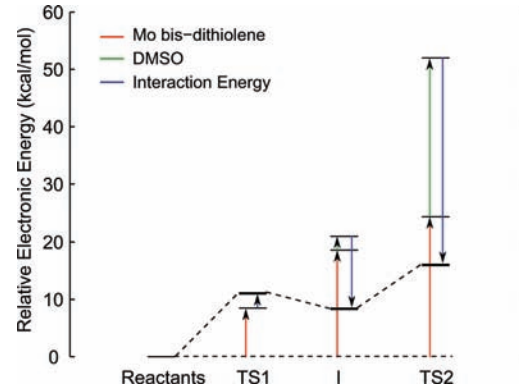


***Figure 6.*** Energetic contributions to the transition states (TS1 and TS2) and DMSO-bound intermediate (I). Distortions of the Mo bis-dithiolene and DMSO fragments are shown in red and green, respectively, and the interaction energy between these fragments is shown in blue.

Mo−O(Me) bond order decreases to 0.6. At the intermediate structure I, the DMSO is still only weakly bound to the Mo complex and the majority of the S−O bond remains intact (bond order of 1.1). Continuing to the second transition state (TS2), the DMSO S−O bond order decreases to 0.7 reflecting the long S−O bond (1.83 Å). The (DMS)O−Mo bond order increases to 0.9, fully compensating the decrease in the DMSO S−O bond order in going from I to TS2. There is also only a minor decrease (∼0.03) in the Mo−O(Me) bond order. Finally, the product Mo(VI)═O and Mo−O(Me) bonds have orders of 1.9 and 0.8, respectively. Therefore, weak Mo−O bond formation begins at the first transition state and oxo transfer (i.e., S−O bond breaking and final Mo−O bond formation) begins around the second transition state.

Fragment calculations, that is, those in which the Mo bis-dithiolene and DMSO are calculated separately using the structures along the reaction coordinate, provide insight into the factors that contribute to the energies of the transition states and the DMSO-bound intermediate. As the DMSO approaches and becomes weakly bound at the intermediate (I, Figure 6), there is a major energetic penalty (∼20 kcal/mol, red) in the Mo complex fragment due to the distortion of the OMe ligand away from the axial position as the complex goes from five- to six-coordinate at the intermediate. This is also reflected in decrease of the Mo−O(Me) bond order from 1.0 in the reactants to 0.6 at the intermediate (Figure 5). In contrast, the energy of the DMSO fragment only slightly increases (∼2 kcal/mol, green) due to longer S−O bond (1.55 Å at the intermediate compared

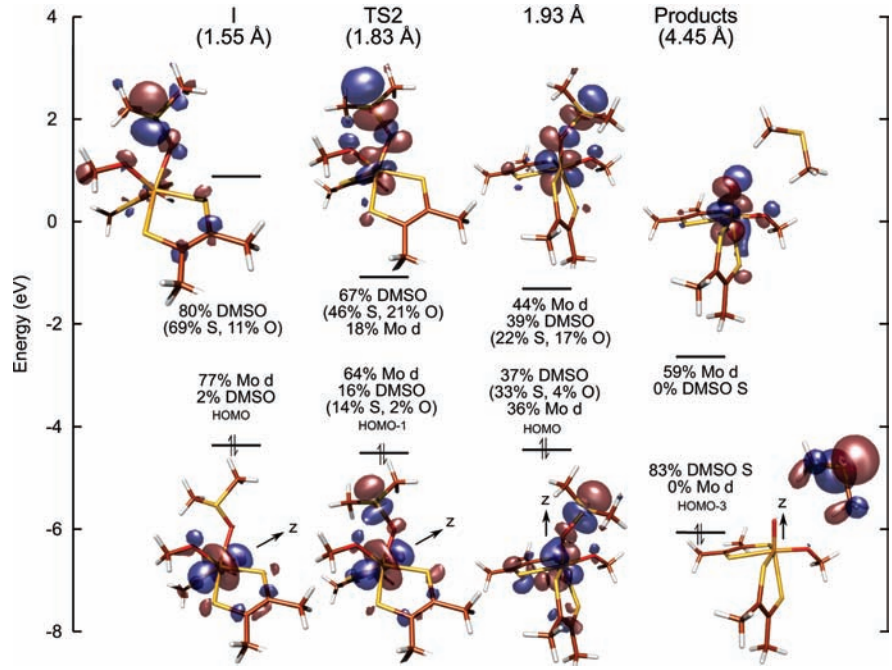


***Figure 7.*** Frontier molecular orbitals involved in oxo transfer, starting from the DMSO-bound intermediate (I), the second transition state (TS2), a point along the S−O breaking coordinate at which the frontier orbitals have equal contributions from DMSO and Mo d (S−O distance of 1.93 Å), and the products with a S−O distance of 4.45 Å. Note that only O and S characters are reported for DMSO because contributions from C and H atoms are minor and that the coordinate system changes in going from I to the products.

to 1.51 Å for free DMSO, Figure 4). The intermediate, however, is stabilized relative to the first transition state (TS1) by ∼10 kcal/mol (blue) due to the bonding interaction between the two fragments. Therefore, the first barrier (i.e., TS1) of the reaction is due the distortion of the OMe ligand and thus can be lowered by decreasing the energetic penalty of this distortion. Indeed, Kirk and co-workers have also demonstrated the energetic cost of this distortion.[19] Additionally, the intermediate can be stabilized by increasing the donor ability of the XO substrate (blue) resulting in a stronger (X)O−Mo bond. Finally, the energy of the second transition state (TS2) has two contributions. The major contribution is from the DMSO fragment due to the significantly increased S−O bond length (1.83 Å compared to 1.55 Å in the intermediate), resulting in an energetic penalty of ∼20 kcal/mol (green). Therefore, the height of the second barrier can be lowered by decreasing the substrate X−O bond strength. Calculations using trimethylamine *N*-oxide (TMNO) demonstrate this effect.[47] There is also a minor energetic penalty (∼5 kcal/mol, red) due to the distortion of the Mo fragment from approximately $D_{3h}$ symmetry at I ($\phi$ = 177.2) toward $O_h$ symmetry ($\phi$ = 156.6) at TS2. This indicates that the height of the second barrier can be also lowered by decreasing the energy required for the distortion toward $O_h$ symmetry.

As discussed above, S−O bond breaking occurs primarily at the second transition state; therefore, additional insight into the mechanism of oxo transfer can be gained by examining the frontier molecular orbitals (FMOs) at and around this transition state (Figure 7). The first structure to be considered is the DMSO-bound intermediate (I, left). Recall that this intermediate is approximately trigonal prismatic and so the filled, nonbonding Mo d orbital lies along the $C_3$ axis and therefore is now labeled as the Mo $d_{z^2}$ orbital. The occupied, donating FMO has 77% Mo d character, predominately from the nonbonding Mo $d_{z^2}$ orbital and 2% DMSO character. The unoccupied, accepting FMO has 85% DMSO character, predominately from the S−O $\sigma$* orbital. Upon going to the second transition state (TS2, left middle), the Mo d character in the donating FMO has decreased to 64% while the DMSO character has increased to 16%. Similarly, the Mo d character in the accepting FMO has increased to 18% while the DMSO character has decreased to 67%. It should be noted again that at this structure, the DMSO bond length has increased from 1.55 to 1.83 Å, which causes the unoccupied S−O $\sigma$* orbital to decrease in energy and become more localized on the oxygen atom, which allows better overlap with the donating FMO (i.e., Mo $d_{z^2}$). As the DMSO S−O distance is systematically increased past TS2 to 1.93 Å, the contributions from Mo- and DMSO-based orbitals to the donating and accepting FMOs are approximately equal. This represents the point "halfway" along the oxo transfer coordinate (S−O distance of 1.93 Å, right middle). It is noteworthy that the ligand field is now better described as $O_h$ ($\phi$ = 110.4°) with the molecular *z*-axis now along the (DMS)O−Mo bond (i.e., the nascent Mo═O axis). The final structure of interest is the product with a S−O distance of 4.45 Å, which is the result of optimizing the products together. Here, the occupied FMO now has 83% DMSO S character and 0% Mo d character, while the unoccupied FMO has 59% Mo d character and 0% DMSO S character.

The orbital compositions at each structure in Figure 7 indicate that at TS2 only about 20% of the electron density has been transferred from the Mo $d_{z^2}$ orbital to the S−O $\sigma$* orbital. Thus, this reaction coordinate is in agreement with an experimental observation that there is no correlation between oxidizability of the metal site and the rate of oxo transfer[17] since the majority of electron transfer occurs after TS2. It should also be noted that calculations using the broken-symmetry formalism were performed for the TS2 structure; however, no wave function

(47) Tenderholt, A. L.; Holm, R. H.; Solomon, E. I. Manuscript in preparation.

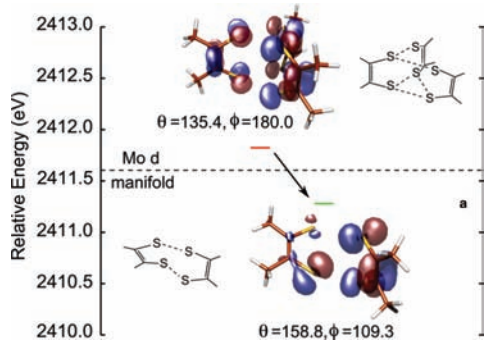


***Figure 8.*** Highest occupied molecular orbitals of the tris- and bis-dithiolene frameworks in $[Mo(mdt)_3]$ and $[MoO(OMe)(mdt)_2]^{1-}$ (left and right, respectively). Note that upon going from the tris- to the bis-dithiolene, there is a distortion away from $D_{3h}$ ($\phi = 180.0°$) toward $O_h$ ($\phi = 109.3°$) symmetry, which decreases the interligand repulsion in addition to having only two dithiolenes.

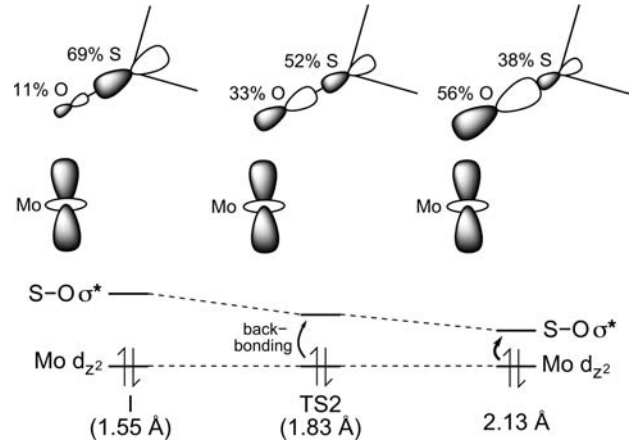


***Figure 9.*** Oxo transfer occurs as a concerted electron transfer mechanism. As the S−O distance is increased along the reaction coordinate, the S−O $\sigma^*$ orbital is stabilized and its O p character is increased, reflecting electron transfer from oxygen to sulfur. These orbital changes further facilitate electron transfer from the molybdenum by increasing the mixing coefficients between the Mo $d_{z^2}$ and S−O $\sigma^*$ orbitals. Note that the orbital compositions are for free DMSO with the indicated S−O distances.

with significant spin-polarization was found. Therefore, oxo transfer involves the occupied Mo $d_{z^2}$ orbital transferring its electrons as a pair to an unoccupied DMSO S−O $\sigma^*$ orbital, which eventually becomes localized as an occupied S p orbital, and is completed after the second transition state.

## 4. Discussion

We consider four major issues concerning oxo transfer in molybdenum enzymes and related model complexes: (1) the innocence or noninnocence of the metal-dithiolene bonding in these sites, (2) the nature of the oxo transfer reaction, (3) the factors contributing to the height of barriers in the oxo transfer reaction coordinate, and (4) the role of the dithiolene in oxo transfer. Each will be discussed using the insight gained from the S K-edge XAS and DFT results of this study.

**4.1. Innocence or Noninnocence of the Dithiolene Ligands.** Our S K-edge XAS and DFT results clearly show that the dithiolenes are innocent in the Mo(VI)═O bis-dithiolene in contrast to formally Mo(VI) tris-dithiolenes (Figure 2b).[6] This could result either from the presence of the oxo ligand or the number of dithiolenes and the geometry of the bis-dithiolene framework (i.e., pseudo-octahedral). Additional calculations show that replacing the oxo with a second OMe ligand only increases the total sulfur character from 224% in $[Mo(OMe)(mdt)_2]^{1-}$ (eight holes) to 256% in $[Mo(OMe)_2(mdt)_2]^{1-}$ (ten holes) for an increase of 32%. While this is more than the change seen in going to $[MoO(OMe)(mdt)_2]^{1-}$ (12%), it is significantly less than the change in S p character in going from $[Mo(mdt)_3]^{2-}$ to $[Mo(mdt)_3]$ (120%). Therefore, the oxo bond is only a minor contribution to the innocence in the Mo bis-dithiolene complex. On the other hand, calculations show that the dithiolene orbital responsible for the noninnocence observed in the tris-dithiolene framework (i.e., $\pi^+_{AB}$) is stabilized in the bis-dithiolene framework by 0.5 eV as a result of a decrease in interligand electron repulsion upon the loss of the third dithiolene and the distortion from $D_{3h}$ ($\phi = 180°$) toward $O_h$ ($\phi = 90°$) symmetry (Figure 8). This stabilization lowers the energy of the dithiolene orbital to below the Mo d manifold, and thus the dithiolenes become innocent. Therefore, the geometry of the ligand environment is primarily responsible for the innocent behavior seen in the Mo(VI)═O bis-dithiolene complex and suggests that mono- and bis-dithiolene complexes of Mo will undergo metal-based oxidation.[48]

**4.2. Nature of Oxo Transfer.** As shown in Figure 7, oxo transfer occurs as the electron pair in the Mo $d_{z^2}$ orbital is transferred to the S p orbital of DMSO to form DMS; however, the nature of this electron transfer as it accompanies the oxo transfer process warrants consideration. There are two hypothetical limiting mechanisms to consider. In formal oxide transfer, the S−O $\sigma^*$ orbital of DMSO (i.e., the LUMO) is mostly localized on the sulfur; oxo coordination to the Mo $d_{z^2}$ orbital provides a superexchange pathway for electron transfer from the molybdenum to the sulfur. In formal oxygen atom transfer, upon elongation of the S−O bond, the S−O $\sigma^*$ orbital localizes on the oxygen and this transfers the electron pair of the oxo to the sulfur; electron transfer would then occur from the Mo $d_{z^2}$ orbital to the oxygen atom. Of course, both S−O elongation and back-bonding of the Mo $d_{z^2}$ orbital into the S−O $\sigma^*$ orbital occur along the reaction coordinate.

At the DMSO-bound intermediate, no significant electron density has been transferred from the Mo $d_{z^2}$ orbital to the S−O $\sigma^*$ orbital, which has only 11% O p character in free DMSO with a S−O bond length of 1.55 Å (left in Figure 9). In going to TS2, the S−O distance increases to 1.83 Å (middle). This increases the O p character in the S−O $\sigma^*$ orbital to 33% in free DMSO and is complimented by an increase in the S p character in the filled S−O $\sigma$ orbital, which indicates that some electron transfer from the oxygen to the sulfur has occurred independent of electron transfer from molybdenum. Also associated with the elongation of the S−O bond at TS2 is the stabilization of the S−O $\sigma^*$ orbital, and thus a bonding interaction with molybdenum becomes possible at the longer S−O distance. Both of these changes in the S−O $\sigma^*$ orbital facilitate backbonding of the electron pair from the Mo $d_{z^2}$ orbital into the S−O $\sigma^*$ orbital by increasing the mixing coefficients, which depend upon their energetic separation and orbital

(48) It should be noted that bis-dithiolene complexes with other metals (such as Ni) undergo ligand-based oxidation due to the larger $Z$ of the metal, which shifts the metal d manifold below the dithiolene ligand valence orbitals in going from Fe to Ni. See ref 5 for more details.

overlap. This increase in O p character continues until the S−O bond is broken. Specifically, for an oxo transfer structure with a S−O distance of 2.13 Å (i.e., S−O bond order 0.15 or 90% broken, right in Figure 9), the S−O $\sigma^*$ orbital in free DMSO has 56% O p character. Therefore, oxo transfer is best described as a concerted process where as the S−O bond is lengthened, the S−O $\sigma^*$ orbital decreases in energy and increases in oxygen character. This allows electrons to be transferred from the molybdenum to the S−O $\sigma^*$ orbital (i.e., oxygen and sulfur) concurrently with electron transfer from the oxygen to the sulfur.

**4.3. Correlation of Oxo Transfer Reaction Coordinate to Kinetics Data.** Before discussing the role of the dithiolene in oxo transfer, we consider the experimental trends observed for oxo transfer to Mo bis-dithiolene model complexes (and their W analogues). This is especially important in order to define and understand the rate-limiting step. Both experimental and calculated reaction coordinates of oxo transfer agree that initial Mo−O bond formation and S−O bond breaking occur at different transition states (i.e., TS1 vs TS2). However, there is disagreement whether the first or second transition state is rate-limiting, and there has been little discussion about the factors that lead to the height of these barriers. Experimental kinetics data indicate that increases in reaction rate due to different substrates (e.g., DMSO, MeNO, PhAsO, etc.) sometimes correlate better with substrate p$K_a$'s and proton affinities than substrate X−O bond strengths.[16] Kinetics data from reactions between $(CH_2)_4SO$ and related $[W(OR')(S_2C_2R_2)_2]^{1-}$ complexes, where $R' = C_6H_5Y'$ and $R = C_6H_5Y$, show that the reaction rate constant increases when substituents Y and Y′ are more electron-withdrawing (i.e., $k_{EWG} > k_{EDG}$; EWG = electron-withdrawing group, EDG = electron-donating group). This is opposite to the expected ease of oxidation of the W(IV) complex.[17] Both of these trends suggest that Mo−O bond formation, and not electron transfer as it accompanies oxo transfer, is the rate-determining step. Calculations, on the other hand, show that the second transition state (TS2, Figure 4) has the largest barrier and therefore is the rate-determining step.[20−22]

The differences between the assignment of rate-limiting steps determined by experimental and computational studies can be reconciled by examining the factors that influence the barriers of the oxo transfer reaction coordinate presented in section 3.3 in the context of the observed trends in oxo transfer to Mo (and W) bis-dithiolenes. It is important to emphasize that in the reaction coordinate in Figure 4, the second transition state (where S−O bond breaking occurs) is the largest barrier with an enthalpy of activation of 16.3 kcal/mol, which is in agreement with kinetics experiments (14.9 kcal/mol).[14] This indicates that TS2 is indeed the rate-determining step for oxo transfer from DMSO to the Mo(IV) bis-dithiolene.

First consider the experimental observation that oxo transfer from substrate is always faster to W complexes compared to their Mo analogues (i.e., $k_W > k_{Mo}$).[12,16] As described in section 3.3, significant S═O bond breaking begins around TS2 as the donating FMO (i.e., Mo $d_{z^2}$) starts to transfer its electron pair to the accepting FMO (i.e., S−O $\sigma^*$); this is observed in Figure 7. The energy of this transition state depends, in part, upon the energetic separation of these orbitals, that is, electron transfer is facilitated as this separation is decreased. This is manifested by the interaction energy between the Mo bis-dithiolene and DMSO fragments in Figure 6 at TS2 (blue line). In going to W, the metal $d_{z^2}$ orbital is destabilized (compared to Mo) due to relativistic effects,[49] which decreases the energetic separation of the FMOs and thus increases the interaction energy. This directly lowers the energy of TS2 (Figure 10a), thereby increasing the rate. Indeed, a computational study determined that the energy of TS2 for oxo transfer using a W bis-dithiolene is lower in energy than that of the analogous Mo bis-dithiolene.[21]

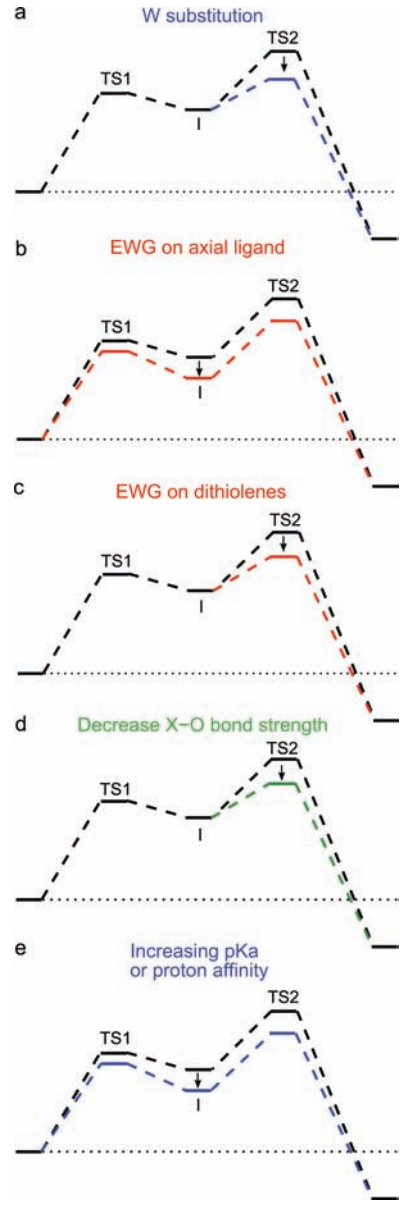


***Figure 10.*** Oxo transfer reaction coordinates as perturbed by (a) substituting Mo with W, (b) adding electron-withdrawing groups (EWGs) to the axial ligand, (c) adding EWGs to the dithiolenes, (d) decreasing substrate X−O strength, or (e) increasing p$K_a$ or proton affinity of substrate.

The second experimental observation to consider is that electron-withdrawing groups on the axial ligand $(O(C_6H_5Y')^{1-})$ increase the rate of oxo transfer.[17] As described in section 3.3, the primary factor controlling the energy of I is the energetic destabilization of the Mo bis-dithiolene fragment (red line at I in Figure 6) due to the distortion and weakening of the Mo−O(Me) interaction. Therefore, decreasing the interaction between the axial OR group and the metal center by adding

(49) Tenderholt, A. L.; Szilagyi, R. K.; Holm, R. H.; Hodgson, K. O.; Hedman, B.; Solomon, E. I. *J. Inorg. Biochem.* **2007**, *101*, 1594–1600.

electron-withdrawing substituents will directly stabilize the intermediate relative to the reactants (Figure 10b). This also indirectly stabilizes TS2 and thus accelerates the reaction.

The third experimental observation is that EWGs on the dithiolene ligands also increase the rate, although not to the same degree as for the axial ligand.[17] It was shown in section 3.3 that a minor contribution (5 kcal/mol) to the energy of TS2 relative to I is the distortion from approximately trigonal prismatic geometry toward octahedral (red line at TS2 in Figure 6). It has also been determined that the energy of this "Bailar twist" is due in part to ligand−ligand repulsion.[6] Therefore, it is expected that adding electron-withdrawing groups, which increases the amount of electron delocalization, would directly lower the energy of TS2, thereby accelerating the rate of oxo transfer (Figure 10c).

The final two experimental observations are that decreasing the X−O bond strength and increasing the p$K_a$ or proton affinity of the substrate accelerates the reaction.[16] First, decreasing the X−O bond strength stabilizes the accepting FMO (far left in Figure 7) relative to the donating FMO so that the X−O bond needs to distort (i.e., lengthen) less for electron transfer to begin. The energetic penalty for this distortion is the primary factor governing the energy of TS2 (green in Figure 6). Therefore, decreasing the X−O bond strength directly lowers the energy of TS2, which increases the rate of oxo transfer (Figure 10d). Second, increasing the p$K_a$ or proton affinity of the XO substrate will stabilize the bound intermediate by increasing the interaction energy between the Mo complex and substrate (blue line in Figure 6). This indirectly decreases the energy of TS2 (Figure 10e) and thus accelerates the reaction.

These five chemical perturbations each directly or indirectly affect the energy of TS2. If certain perturbations are added to the system, it is possible to shift the rate-determining step from TS2 to TS1. Indeed, a previous computational study of oxo transfer from DMSO to a W(IV) bis-dithiolene complex calculated that TS1 is ∼1 kcal/mol higher in energy than TS2.[21] Similarly, calculations of oxo transfer using MeNO as a substrate also indicate that TS1 is the largest barrier and thus the rate-limiting step.[47]

**4.1. Role of the Dithiolene in Oxo Transfer.** An important role of the dithiolene in oxo transfer to Mo(IV) des-oxo sites appears to be to stabilize a singlet ground state (as opposed to a triplet state) in the reactants. Mo(IV) complexes without oxo groups often have triplet ground states due to the limited splitting of the Mo $d_\pi$ orbitals.[50−52] However, for the dithiolene ligands, the C═C bond orients the sulfur out-of-plane p orbitals, creating $\pi$ anisotropy such that only the Mo $d_{xz}/d_{yz}$ orbitals can interact with these ligand orbitals (Figure 11). This anisotropy destabilizes the Mo $d_{xz}/d_{yz}$ orbitals relative to the Mo $d_{x^2-y^2}$ orbital ($x$ and $y$ axes bisect the Mo-ligand bonds), which results in a stabilized singlet ground state in the Mo(IV) des-oxo site. Calculations indicate a splitting of the Mo $d_\pi$ orbitals greater than about 0.6 eV is required to overcome the $d^2$ electron repulsion and spin pair (Figure S5 in Supporting Information). This stabilization of the singlet ground state in the Mo(IV) des-oxo complex persists along the oxo transfer reaction coordinate

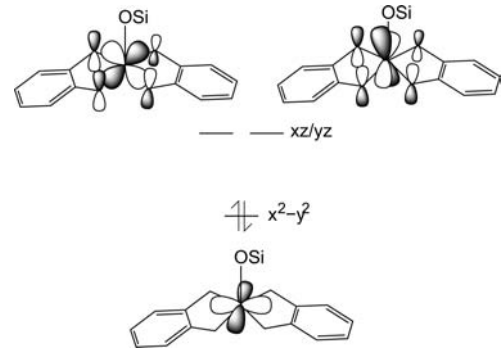


***Figure 11.*** C═C double bond of the dithiolene orients the sulfur out-of-plane p orbitals, creating $\pi$ anisotropy, which stabilizes the singlet ground state.

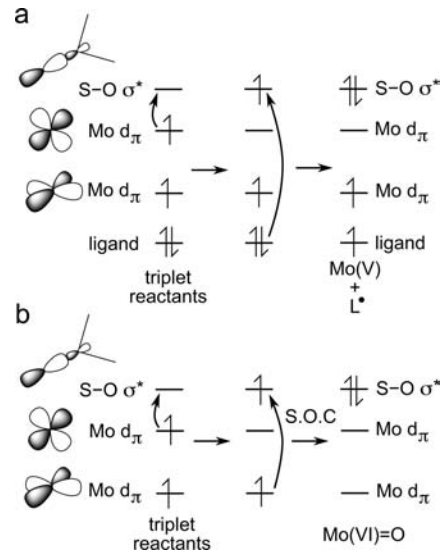


***Figure 12.*** (a) Triplet reactant results in an unfavorable Mo(V) site with a ligand radical, and (b) intersystem crossing between the triplet and singlet surfaces is inefficient due to poor spin−orbit coupling (SOC).

(Figure S6 in Supporting Information) and is important in the oxo transfer reaction for two reasons.

First, the mechanism of oxo transfer from DMSO requires that two electrons be transferred to the S−O $\sigma^*$ orbital. For a singlet Mo(IV) des-oxo complex, this involves an electron pair in the Mo $d_{z^2}$ orbital (using the coordinates of the trigonal prismatic DMSO-bound intermediate) being transferred to the S−O $\sigma^*$ orbital. In the case of a triplet reactant, two Mo $d_\pi$ orbitals are occupied in the α manifold; however, only one of these orbitals can directly transfer its electron to the S−O $\sigma^*$ orbital. The second electron must come from the $\beta$ manifold, but since all of the $\beta$-spin Mo d orbitals are unoccupied, this electron is transferred from a ligand-based orbital (Figure 12a). This would result in a Mo(V) site with a ligand radical which is unstable by ∼10 kcal/mol relative to the closed-shell Mo(VI)═O site created from the singlet reactant (products in Figure S6 in Supporting Information).

Second, intersystem crossing between singlet and triplet states requires efficient spin−orbit coupling from an occupied α orbital to an unoccupied $\beta$ orbital. Since spin−orbit coupling is dominately a single-center operator, efficient spin−orbit coupling requires that these orbitals be mostly localized on the same atom. However, the singlet and triplet surfaces cross late along the oxo transfer reaction coordinate for reactions involving a

(50) Sarkar, S.; Carlson, A.; Veige, M.; Falkowski, J.; Abboud, K.; Veige, A. *J. Am. Chem. Soc.* **2008**, *130*, 1116–1117.
(51) Most, K.; Mosch-Zanetti, N.; Vidovic, D. *Organometallics* **2003**, *22*, 5485–5490.
(52) Schrock, R.; Seidel, S.; Mösch-Zanetti, N.; Shih, K.; O'Donoghue, M.; Davis, W.; Reiff, W. *J. Am. Chem. Soc.* **1997**, *119*, 11876–11893.

triplet Mo(IV) complex such as $[Mo(OMe)Cl_4]^{1-}$ (Figure S7 in Supporting Information). In this reaction, the occupied α orbital is metal-based while the unoccupied $\beta$ orbital has mostly S−O $\sigma^*$ character, and thus spin−orbit coupling between these two states is inefficient (Figure 12b). Indeed, calculations for oxo transfer to the triplet complex $[Mo(OMe)Cl_4]^{1-}$ show that the electron transmission coefficient from the triplet to singlet surfaces is small at the crossing point (Figure S8 in Supporting Information) and strongly depends upon the metal character in the involved orbitals (Figure S9 in Supporting Information).

It should be noted that these results differ from a recent study of isoelectronic (i.e., metal $d^2$ configuration) V, Nb, and Ta complexes.[53] First, oxo transfer to $[Mo(OMe)(mdt)_2]^{1-}$ involves only a singlet ground state along the reaction coordinate since the triplet states are higher in energy. This is in contrast to the V complexes studied by Wolczanski, Cundari, and co-workers in which the reactants and their substrate-bound intermediates have triplet ground states. Second, Wolczanski, Cundari, and co-workers propose that oxo transfer from $R_3PO$ and (silox)-WNO (silox = $^tBu_3SiO$) to these complexes occurs through a substrate-bound intermediate in a triplet electronic state to avoid electron repulsion between the filled M $d_{z^2}$ orbital and the substrate E−O $\sigma$ orbital. This electron repulsion, however, is less of an issue for the Mo(IV) bis-dithiolene complex as the DMSO substrate does not directly approach the filled Mo $d_{z^2}$ orbital (see Figure 7). Finally, the conservation of orbital symmetry seen for the tetrahedral V complexes does not extend to the Mo bis-dithiolene system since the geometry of the DMSO-bound intermediate (trigonal prismatic) is different from that of the Mo(VI)═O product (octahedral).

## 5. Conclusions

The electronic structures of a set of Mo(IV) and Mo(VI)═O bis-dithiolene complexes have been determined using our S K-edge XAS and DFT methodology. These results indicate that the dithiolene ligands behave innocently, that is, the Mo(IV) complex undergoes metal-based oxidation due to the structure of the bis-dithiolene framework that limits ligand−ligand repulsion and not the presence of a strong axial oxo ligand in the six-coordinate Mo(VI) complex. These experimentally validated DFT calculations were then extended to determine the reaction coordinate of oxo transfer from DMSO to the Mo(IV) bis-dithiolene, indicating that the reaction proceeds through a DMSO-bound intermediate. Insight into the factors that control the enthalpies of activation for the transition states and intermediate is provided by fragment calculations. Specifically, the enthalpy of the intermediate has contributions from both the energy required to distort the Mo(IV) bis-dithiolene to accommodate the substrate and the interaction energy between the substrate and Mo complex, while the enthalpy of the second transition state (TS2) is predominately affected by the strength of the substrate X−O bond. Examination of the electronic structures around TS2 indicate that DMSO S−O bond breaking occurs after this state. The nature of this oxo transfer process requires the elongation of the S−O bond, which stabilizes the S−O $\sigma^*$ orbital and increases its oxygen character. This allows for better mixing between the Mo $d_{z^2}$ and the S−O $\sigma^*$ orbitals and facilitates electron transfer from the molybdenum to the sulfur atom. Comparison of the reaction coordinate with kinetics data provides additional insight into the effects various perturbations have on the rate of oxo transfer via the direct stabilization of either the intermediate or TS2. These perturbations include W substitution, presence of electron-withdrawing groups on the axial alkoxyl or dithiolene ligands, and use of a different substrate. Finally, the role of the dithiolene in stabilizing a singlet ground state of the Mo(IV) des-oxo site and its importance in the oxo transfer reaction are discussed.

**Acknowledgment.** This work was supported by NSF CHE 0446304 (E.I.S.), NIH RR-001209 (K.O.H.), NSF CHE 0547734 and CHE 0846397 (R.H.H.). SSRL operations are funded by the Department of Energy, Office of Basic Energy Sciences. The SSRL Structural Molecular Biology program is supported by the National Institutes of Health, National Center for Research Resources, Biomedical Technology Program and by the Department of Energy, Office of Biological and Environmental Research. This publication was made possible by Grant Number 5 P41 RR001209 from the National Center for Research Resources (NCRR), a component of the National Institutes of Health (NIH).

**Supporting Information Available:** Complete citation for ref 28; representative fits to the normalized and second derivative S K-edge data of $[Mo(OSi)(bdt)_2]^{1-}$ and $[MoO(OSi)(bdt)_2]^{1-}$ complexes; comparison of structural parameters between geometry optimized (DFT) and crystallographic structures of $[Mo(OSi)(bdt)_2]^{1-}$ and $[MoO(OSi)(bdt)_2]^{1-}$; detailed molecular orbital compositions of these complexes; comparisons of electronic and geometric structures for $[Mo(OSi)(bdt)_2]^{1-}$/$[Mo(OMe)(mdt)_2]^{1-}$ and $[MoO(OSi)(bdt)_2]^{1-}$/$[MoO(OMe)(mdt)_2]^{1-}$; MO diagram showing $d_\pi$ splittings; comparison of the singlet and triplet oxo transfer reaction coordinates; triplet and singlet surfaces for oxo transfer to $[Mo(OMe)Cl_4]^{1-}$, and the derivation and calculation of the electron transmission coefficient to move between these surfaces; Cartesian coordinates for all optimized structures (zipped XYZ files). This material is available free of charge via the Internet at http://pubs.acs.org.

JA910369C

(53) Veige, A.; Slaughter, L. M.; Lobkovsky, E. B.; Wolczanski, P. T.; Matsunaga, N.; Decker, S. A.; Cundari, T. R. *Inorg. Chem.* **2003**, *42*, 6204–6224.